Available online at www.sciencedirect.com
ScienceDirect
Trans. Nonferrous Met. Soc. China 30(2020) 1227−1237
Transactions of Nonferrous Metals Society of China
www.tnmsc.cn

Effects of pre-deformation mode and strain on creep aging bend-forming process of Al−Cu−Li alloy

Jian-guo TANG[1], Bo YU[1], Jin ZHANG[1,2], Fu-shun XU[3,4], Chong-jun BAO[3,4]

1. Light Alloy Research Institute, Central South University, Changsha 410083, China;
2. State Key Laboratory of High Performance and Complex Manufacturing, Central South University, Changsha 410083, China;
3. Kunming Metallurgical Research Institute, Kunming 650031, China;
4. State Key Laboratory of Pressure Hydrometallurgical Technology of Associated Nonferrous Metal Resources, Kunming 650031, China

Received 30 July 2019; accepted 15 April 2020

Abstract: The bending deformation method was adopted to characterize the creep deformation behavior of Al−Cu−Li alloy in the creep aging forming (CAF) process based on a series of CAF tests, and the evolution laws of its mechanical properties and microstructures under different pre-deformation conditions were studied. The results show that the bending creep strain characterization method can intuitively describe the creep variation. With the increase of the pre-deformation strain, the creep strain of the specimen firstly increases and then decreases. The increase of the pre-deformation strain can promote the course of aging precipitation, and improve the formed alloy's tensile properties at room temperature, the Kahn tearing properties, and the fatigue propagation properties. Pre-rolled specimens produce a slightly weaker work hardening than pre-stretched specimens, but they also create a stronger aging-strengthening effect; thus the strength, toughness and damage performance can be improved to some extent. Among all the types of specimens, the specimen with 3% rolling after CAF treatment has the best comprehensive mechanical properties.

Key words: Al−Cu−Li alloy; creep aging forming; pre-deformation; bending creep strain; microstructure evolution; mechanical properties

1 Introduction

The creep aging forming (CAF) process is an advanced forming technique developed for manufacturing integral wing panels from high-strength aluminum alloy [1,2]. An aluminum alloy workpiece, under loading stress within the elastic limits and aging temperature, synchronously experiences creep deformation and aging strengthening, and the forming target can be achieved at the end of the aging treatment [3]. By virtue of its low density, high specific stiffness, high specific strength, and other superior properties, Al−Cu−Li alloy has been seen as an ideal choice for aerospace structures [4−7]. The mechanical properties of Al−Cu−Li alloys depend to a large extent on the fine precipitates formed in the aging process, including the δ'-Al_3Li, θ'-Al_2Cu, and T_1-Al_2CuLi phases [8−10]. Among them, the T_1 phase has the best strengthening effect [11]. Before artificial aging of Al−Cu−Li alloy, dislocation is usually introduced via pre-deformation to promote massive nucleation, thereby enhancing aging strengthening [12−15]. According to the findings of CASSADA et al [12], the pre-deformation of

Foundation item: Project (2017YFB0306301) supported by the National Key Research and Development Program of China; Project (51705539) supported by the National Natural Science Foundation of China
Corresponding author: Jin ZHANG, Tel: +86-731-88876913, E-mail: zhangjinlari@csu.edu.cn;
Fu-shun XU, Tel: +86-731-88830265, E-mail: xuzhang1808@163.com
DOI: 10.1016/S1003-6326(20)65291-8

Al−Cu−Li alloy before aging reduces the thickness and length of the T_1 phase, increases the number density by nearly two orders of magnitude, and improves the yield strength by about 100 MPa. Furthermore, the study by GABLE et al [13] reveals that pre-deformation influences the competitive precipitation kinetics behavior of the precipitated phase in Al−Cu−Li alloy, and that the increase of the pre-deformation strain further increases the relative volume fractions of the T_1 phase and the θ' phase and further improves the yield strength of the alloy. In the study by LIN et al [14] on Al−Cu−Li alloy, relative to the T6 state, the T8 state acquires fine and dispersed δ' and T_1 phases, as well as the interrupted intergranular phase, and the tensile properties are correspondingly improved. The findings of ZHANG et al [15] revealed that low-level pre-deformation not only improves the strength of Al−Cu−Li alloy, but also enhances its fracture toughness. The study by LIU et al [16] on Al−Cu−Li alloy makes clear that different pre-deformation modes and strains lead to different texture types, and that, relative to the alloy without pre-deformation, the pre-deformed alloys have more Goss texture components and thus feature a higher fatigue damage tolerance.

Both pre-stretching and pre-rolling are pre-deformation modes commonly adopted for aluminum alloy before aging. Pre-stretching enhances the material's strength, and stretches and straightens formed parts; however, due to the small plastic zone size and the weak fracture closure effect, it weakens the resistance of alloy sheets to fatigue crack propagation (FCP) [17]. In contrast, moderate pre-rolling enjoys certain advantages in elevating the damage tolerance of aluminum alloy [18]. For instance, by adopting a small pre-rolling deformation (6.1%), HUANG et al [19] successfully improved the damage tolerance of Al−Cu−Mg alloy plates. This study focuses on the basic research of creep aging forming technology for single-curvature aerospace components. Existing studies on the evolution of the creep aging process usually adopt the uniaxial creep tension and compression test method; however, because of the stress characteristics of panels in the bending formation process (i.e., tension on the convex side, and compression on the concave side), the creep strain−time curve obtained by the uniaxial creep test method cannot reflect the actual bending deformation (that is, the overall deformation effect created by the continuous variation of the plastic strain on the thickness section) [20−22]. In this case, the only resort is an actual deformation test on the panels, such as a CAF test on bending molds with a curved profile [22−26]. For this consideration, in this work a bending CAF experiment on panels was performed, hoping to characterize the bending creep deformation laws of panels with bending deflection. By investigating the influence laws of different pre-deformation modes and strains on the CAF bending process of Al−Cu−Li alloy panels, a scientific reference was offered for applying the creep aging of Al−Cu−Li alloy.

2 Experimental

2.1 Materials

Table 1 provides the chemical composition of hot-rolled thick plate of 2050 Al alloy, i.e., the material used in this study. After receiving the solution treatment (510 °C, 1 h), the alloy was quenched at room temperature, followed by pre-deformation treatments along the panel rolling direction (i.e., 0%, 3% stretching, 3% rolling, 9% stretching, and 9% rolling). The pre-stretching and pre-rolling experiments were completed on a room-temperature tensile testing machine and a cold-rolling mill, respectively. To avoid the influence of thickness deviation, the pre-deformed samples were specially machined and trimmed into a uniform size. The sizes of specimens used for CAF experiment were as follows: the specimen size used for the mechanical properties test and microstructure sampling was 140 mm × 40 mm × 3 mm; the size used for the deflection test was 140 mm × 20 mm × 3 mm. A smaller width was selected for the latter, mainly to reduce the influence of the processing precision on the measurement error in the width direction and to save material.

Table 1 Chemical composition of 2050 Al alloy (wt.%)

Cu	Li	Mn	Ag	Mg	Zr
3.24	0.83	0.38	0.35	0.32	0.083

Zn	Ti	Fe	Si	Al
0.053	0.038	0.045	0.053	Bal.

2.2 Bending CAF experiment

Figure 1 shows a self-made bending deformation mold with a curvature radius of 1000 mm, used for the CAF bending experiment. Firstly, the specimen was placed at the center of the lower half of the mold, while the upper half was placed on the specimen's surface. After confirming the strict alignment between the upper half and the lower half, the screws were tightened until the specimen fully fitted the mold, and the pressure was maintained for 15 min. Then, the assembly was put inside an aging furnace, and, when the furnace temperature rose to 160 °C, thermal insulation was provided for different periods. The total testing time of 60 h was chosen to ensure a complete evolution, while also ensuring the aging strengthening of all near the peak state. Figure 2 shows the schematic diagram of CAF. The maximum deflection f of the workpiece was measured after the specimen was taken out at different time nodes in the creep aging process. Referring to the bending strain formula of pure bending [27] and the geometric relationship between curvature radius and defection, as shown in Eq. (1) and Eq. (2) respectively, the creep strain ε_f occurring in the bending deformation process can be defined as Eq. (3):

$$\varepsilon = \frac{h}{2r} \tag{1}$$

$$r = \frac{f}{2} + \frac{L^2}{8f} \tag{2}$$

$$\varepsilon_f = \frac{4fh}{4f^2 + L^2} \tag{3}$$

where ε denotes the bending strain; h denotes the specimen's thickness; r denotes the curvature radius; L denotes the span.

Fig. 1 Photo of single-curvature CAF mold

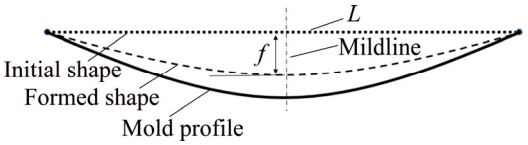

Fig. 2 Schematic diagram of CAF

2.3 Mechanical properties tests and microstructure observation

The mechanical properties of the alloys at room temperature and different time nodes were measured to obtain the creep aging strength variation curve. A room-temperature tensile test was performed on a CSS−44100 testing machine at a tensile speed of 2 mm/min. Peak aged samples at different pre-deformation states were put through the Kahn tearing test and the FCP test. As specified in ASTM B871—01, the tearing properties were tested on a CSS−44100 testing machine at a test speed of 1.5 mm/min, and the samples taken from the hot-rolled sheet in L−T orientation were prepared. Related parameters include the unit initial energy (UIE, the energy dissipated before crack propagation), and the tearing strength (TS). The fatigue test was conducted on an MTS Landmark testing machine according to ASTM 647—00. In the test the sinusoidal cyclic constant load was adopted with a stress ratio of 0.1 ($R=\sigma_{min}/\sigma_{max}$) and a frequency of 10 Hz, and the cracking direction was vertical to the rolling direction; the stress intensity factor ΔK at the tip of the pre-crack, 1 mm in size, was 9 MPa·m$^{1/2}$. Prior to the start of the mechanical properties test, the specimens were straightened by pre-stretching to remove curviness of the formed samples. The sizes of three kinds of samples used for mechanical properties testing are shown in Fig. 3.

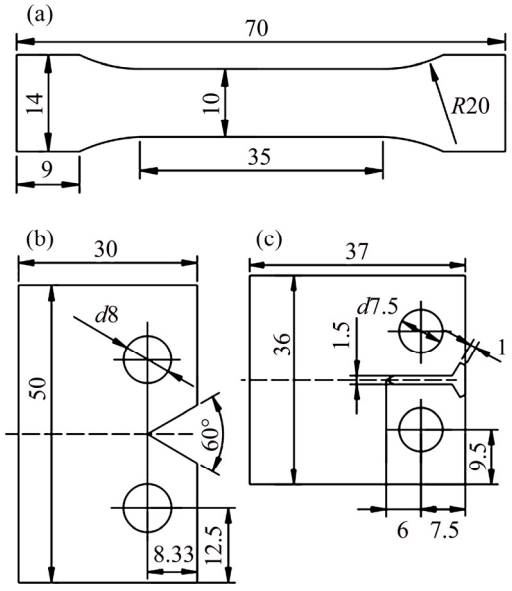

Fig. 3 Samples for mechanical properties testing (unit: mm): (a) Room-temperature tensile test; (b) Kahn tear test; (c) Fatigue crack growth test

Fatigue fracture was observed with a ZEISS EVO MA10 scanning electron microscope. The specimen used for the TEM microstructure observation was mechanically ground to a thickness of 80 μm, and cut into discs with 3 mm in diameter. After that the solution prepared with 20% nitric acid and 80% methanol at −20 °C and 20 V was used for electropolishing. The microstructure characteristics were characterized using an FEI Titan F20G2 at a working voltage of 200 kV.

3 Results and discussion

3.1 Laws of bending creep strain

Figure 4 shows the bending creep strain−creep aging time curves of the AA2050 alloy under different creep aging regimes. As can be seen from the common trends of different curves, the creep law of the pure bending creep samples in the state of stress relaxation can be divided into two stages. The creep strain rate gradually declines in the first stage, and then the creep strain becomes closer to saturation in the second stage. Moreover, the first stage of pre-deformed samples is longer, and a larger cumulative strain can be obtained with less holding time under the corresponding conditions. At the end of the first stage (about 24 h), the total creep strain has accumulated to a high level, and the subsequent increment is small. Compared with the case without pre-deformation, the creep strain of the pre-deformed specimen at the same time node is much higher. Figures 4(a) and (b) show the influence of the pre-deformation strain on the creep strain of the specimens. Clearly, with the increase of pre-deformation strain, no matter in terms of stretching or rolling, the bending creep strain uniformly manifests a trend of first increasing and then decreasing. For instance, after the CAF treatment for 10 h, the creep strain of the pre-deformed specimen is about twice of that of a specimen without pre-deformation; the creep strain of the specimen under 9% pre-deformation is slightly lower than that of the specimen under 3% pre-deformation. According to Figs. 4(c) and (d), in the creep aging process, the pre-rolled and pre-stretched specimens, pre-deformed to the same

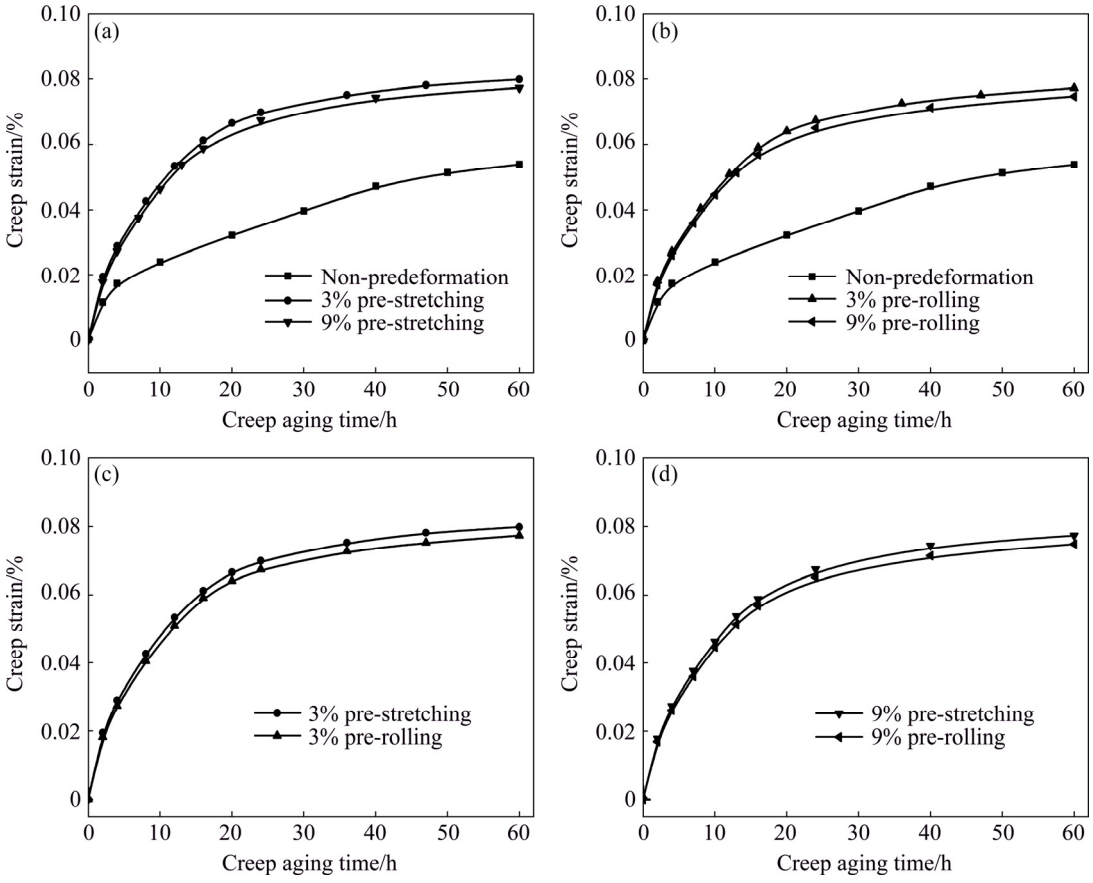

Fig. 4 Effect of pre-deformation on evolution of creep strain during creep aging: (a) Effect of pre-stretching strain; (b) Effect of pre-rolling strain; (c) Effect of pre-deformation mode with strain of 3%; (d) Effect of pre-deformation mode with strain of 9%

strain, show similar creep laws, and the creep strain value of the former is slightly less than that of the latter. It takes different periods of time for the five types of specimens to reach their peak strengths, so the factors influencing the total creep strain of the specimens include both the pre-deformation and the CAF time. For these five types of specimens (i.e., non-predeformed, 3% pre-stretching, 9% pre-stretching, 3% pre-rolling, and 9% pre-rolling), the total creep strain values are 0.0538%, 0.0699%, 0.0598%, 0.0674% and 0.0567%, respectively. As indicated by the results, when the five types of specimens are at their peak strengths, the specimen with 3% pre-deformation has the highest total creep strain value, while the total strain creep value of the specimen with 9% pre-deformation is slightly higher than that of the specimen without pre-deformation.

In the above results, although there are no obvious gaps between different pre-deformation modes (Figs. 4(c, d)) with the same pre-deformation strain, the differences can be magnified many times in the corresponding bending radii. The mathematical relationship between bending creep strain and final curvature radius ($r=h/(2\varepsilon)$) is drawn into a curve as shown in Fig. 5. The related forming region of all the samples, which locates at the leftward curve segment with a higher slope, has been marked in the figure. It can be seen that, in this range, slight difference of the creep strain can be more intuitively reflected by the difference of the forming radius. For example, the curvature radii of 9% pre-stretched and 9% pre-rolled samples after creep forming are 2.540 and 2.645 mm, respectively.

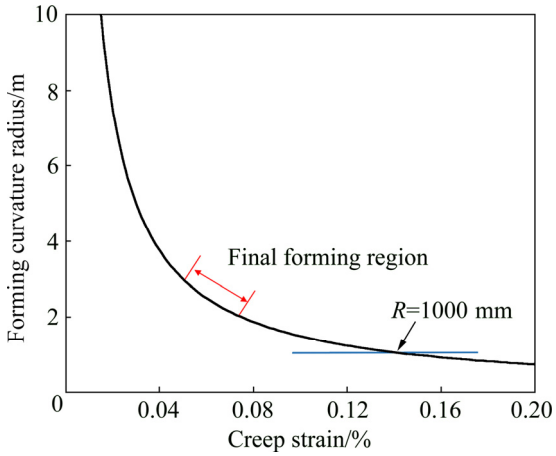

Fig. 5 Relationship between forming curvature radius and creep strain

3.2 Tensile and Kahn tear properties

Figure 6 shows the yield strength variation curves of different pre-deformed alloys during the creep aging process. Clearly, with the increase of the creep aging time, the yield strength of the alloys is also gradually improved, manifesting an obvious aging-strengthening characteristic. Pre-deformation before creep aging significantly shortens the aging time required for the alloy's strength to reach its peak state. To be specific, the alloy without pre-deformation reaches its peak strength after 60 h of creep aging at 160 °C; in contrast, the alloys with 3% and 9% pre-deformation (stretching and rolling) before creep aging are basically in their peak strength states at 24 and 16 h, respectively. Meanwhile, introducing pre-deformation can improve the peak strength of the alloys after creep aging. As shown in Fig. 7(a), relative to the alloy without pre-deformation, the alloy with 3% pre-stretching shows an improvement in its peak strength by about 40 MPa after creep aging. However, there is no significant difference (only about 10 MPa) between the alloy with 3% pre-stretching and that with 9% pre-stretching after creep aging. For simplicity, the strength contribution after creep aging of the alloy in this study is divided into three components [28]:

$$\sigma_y=\sigma_b+\sigma_s+\sigma_p \quad (4)$$

where σ_y is the yield strength of the material, σ_b is the base strength of the matrix and the solid solution, and σ_s and σ_p represent the strength increase caused by strain hardening and precipitation strengthening, respectively. With the increase of the pre-deformation strain, the work

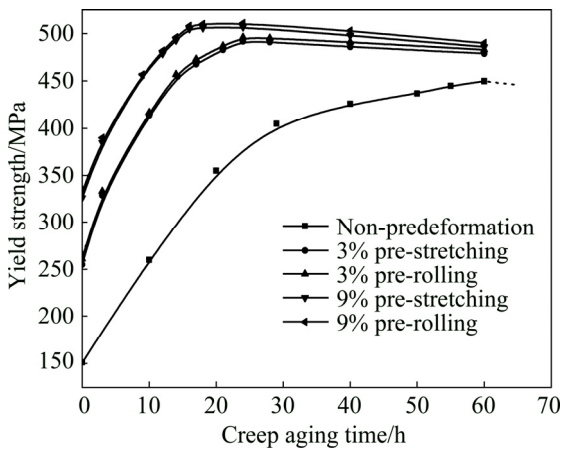

Fig. 6 Effect of pre-deformation on yield strength evolution of samples during creep aging process

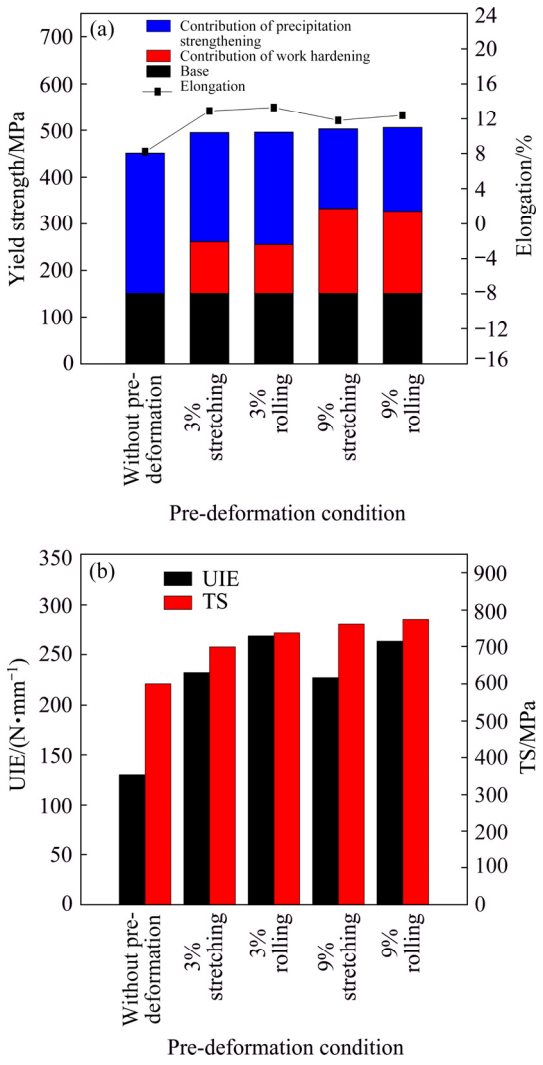

Fig. 7 Effect of pre-deformation on mechanical properties of samples in peak strength states: (a) Tensile properties at room temperature; (b) Kahn tearing properties

hardening of the alloys is improved as well, but the improvement rate declines with the increase of the pre-deformation strain. The strength contribution of the precipitated phase declines with the increase of the pre-deformation strain. For instance, for the specimens with 3% and 9% pre-stretching, the strength contributions of the precipitated phase, which can be estimated by the difference between the yield strength at the pre-stretched state and the subsequent creep aged state, are 234 and 171 MPa, respectively. For the alloy with 9% pre-deformation, the strength contribution of the work hardening is approximately equal to that of the precipitation strengthening. The weakening of the precipitation strengthening with the increase of the pre-deformation strain is attributed to the comprehensive influence of the precipitated phase type, size and density [28]. According to the columnar data in Fig. 7(a), for the same pre-deformation strain, the pre-stretched specimens, relative to the pre-rolled specimens, have a slightly stronger work hardening effect and a weaker precipitation strengthening effect, but the difference is insignificant (uniformly within 10 MPa). As a result, their strength variation curves almost overlap each other.

Figure 7(b) shows the Kahn tearing property charts of five creep aging specimens, where UIE and TS denote the unit initiation energy (fracture toughness) and the tear strength, respectively. Through observing the experimental data on UIE and TS, it is found that, relative to the specimens without pre-deformation, the pre-deformed samples all show some increase in the UIE and TS values after creep aging. There is a good correspondence between the variation trend of the TS value and the tensile strength at room temperature. With the increase of the pre-deformation strain, the UIE value first greatly increases, and then slowly declines. Relative to the UIE value of the specimen without pre-deformation (130 N/mm), the UIE values of the specimens with 3% pre-stretching and 3% pre-rolling increase by 78.5% and 106.9%, and reach 232 and 269 N/mm, respectively. The UIE values of the specimens decline slightly from 3% pre-deformation to 9%, and the UIE values of the specimens with 9% pre-stretching and pre-rolling are 227 and 263 N/mm respectively, with a rate of decline of less than 10% in each case. With the same pre-deformation strain, the UIE values of the pre-rolled specimens are higher than those of the pre-stretched specimens; relative to the specimens with 3% and 9% pre-stretching, the pre-rolled specimens show an increase of about 16% in their UIE values. Clearly, pre-rolling deformation can improve the fracture toughness of the alloys to some extent, but excessive pre-rolling (9%), on the contrary, will reduce the fracture toughness of the alloys.

3.3 Fatigue resistance property

Figure 8 shows the FCP rate of the Al−Cu−Li alloy after creep aging under different pre-deformation modes and strains. The FCP rate for the five types of specimens increases with the

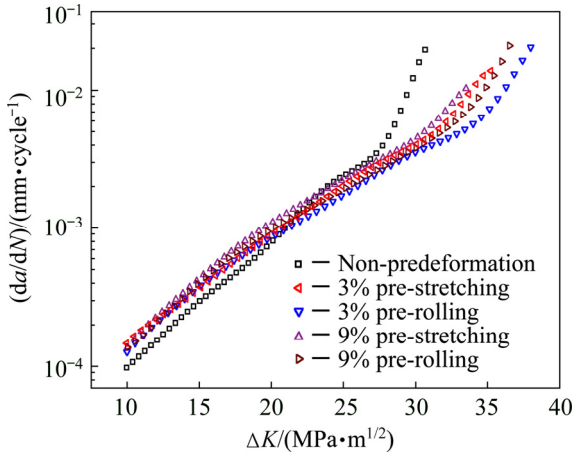

Fig. 8 Effect of pre-deformation on FCP curves of samples in peak strength states

increase of the stress intensity factor ΔK. The four types of the pre-deformed specimens are obviously different from the specimen without pre-deformation in the increasing trend of the FCP rate. With the progress of the FCP rate, the pre-deformed alloys show a higher FCP rate; however, in the vicinity of ΔK=22 MPa·m$^{1/2}$, the results are reversed. It should be noted that, relative to the specimens without pre-deformation, the pre-deformed specimens have higher ΔK values, suggesting that introducing pre-deformation will help to improve the damage tolerance of alloys. Under the same deformation strain, compared to the pre-stretched specimens, the pre-rolled specimens show lower da/dN values (a is the length of crack; N is the number of cycles) and higher ΔK values, that is, higher crack propagation resistance and damage tolerance. This is related to the protected compressive stress gradient produced in the pre-rolling deformation process of the alloys [18]. In addition, regardless of pre-stretching or pre-rolling, the specimens with 3% pre-deformation have a lower FCP rate and higher damage tolerance than those with 9% pre-deformation after creep aging, suggesting that excessive pre-deformation will be detrimental to the damage tolerance of the alloys, which is consistent with the results of existing studies [18,19].

Figure 9 shows fatigue fracture morphologies of different pre-deformed alloys after CAF in the

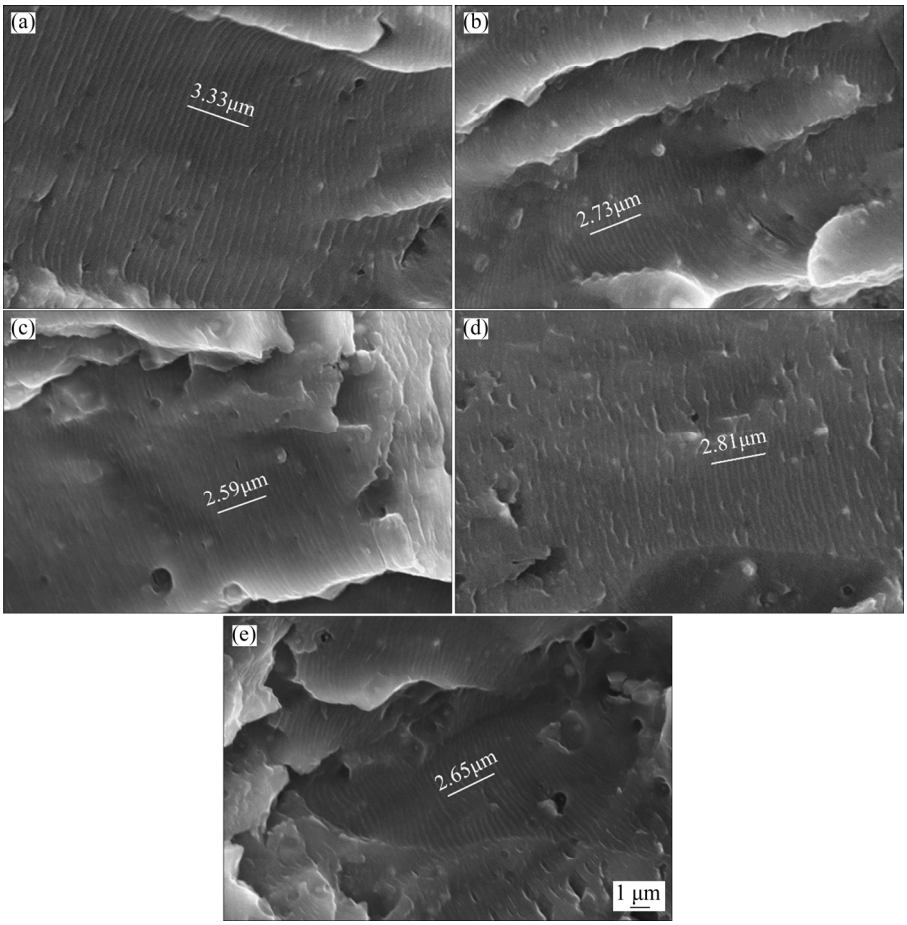

Fig. 9 Effect of pre-deformation on fatigue fracture morphologies of samples in paris stage (ΔK=25 MPa·m$^{1/2}$): (a) Without pre-deformation; (b) 3% pre-stretching; (c) 3% pre-rolling; (d) 9% pre-stretching; (e) 9% pre-rolling

Paris stage (ΔK=25 MPa·m$^{1/2}$). It displays the propagation paths and striation zones of fatigue cracks under cyclic stress, and marks the widths of ten striations. Usually, a greater striation width means a higher FCP rate and a reduced crack propagation resistance. According to the widths of the striations marked in Fig. 9, the crack propagation resistance from high to low can be ranked as follows: 3% pre-rolling > 9% pre-rolling > 3% pre-stretching > 9% pre-stretching > non-predeformation. Apparently, for the five types of specimens at their peak strengths, the CAF specimen of Al−Cu−Li alloy treated with a smaller deformation strain (3% pre-rolling) has the highest fatigue resistance.

3.4 TEM microstructures

Figure 10 shows the bright field TEM images, SAED patterns and T_1 phase HRTEM image of Al−Cu−Li alloy with different creep aging regimes

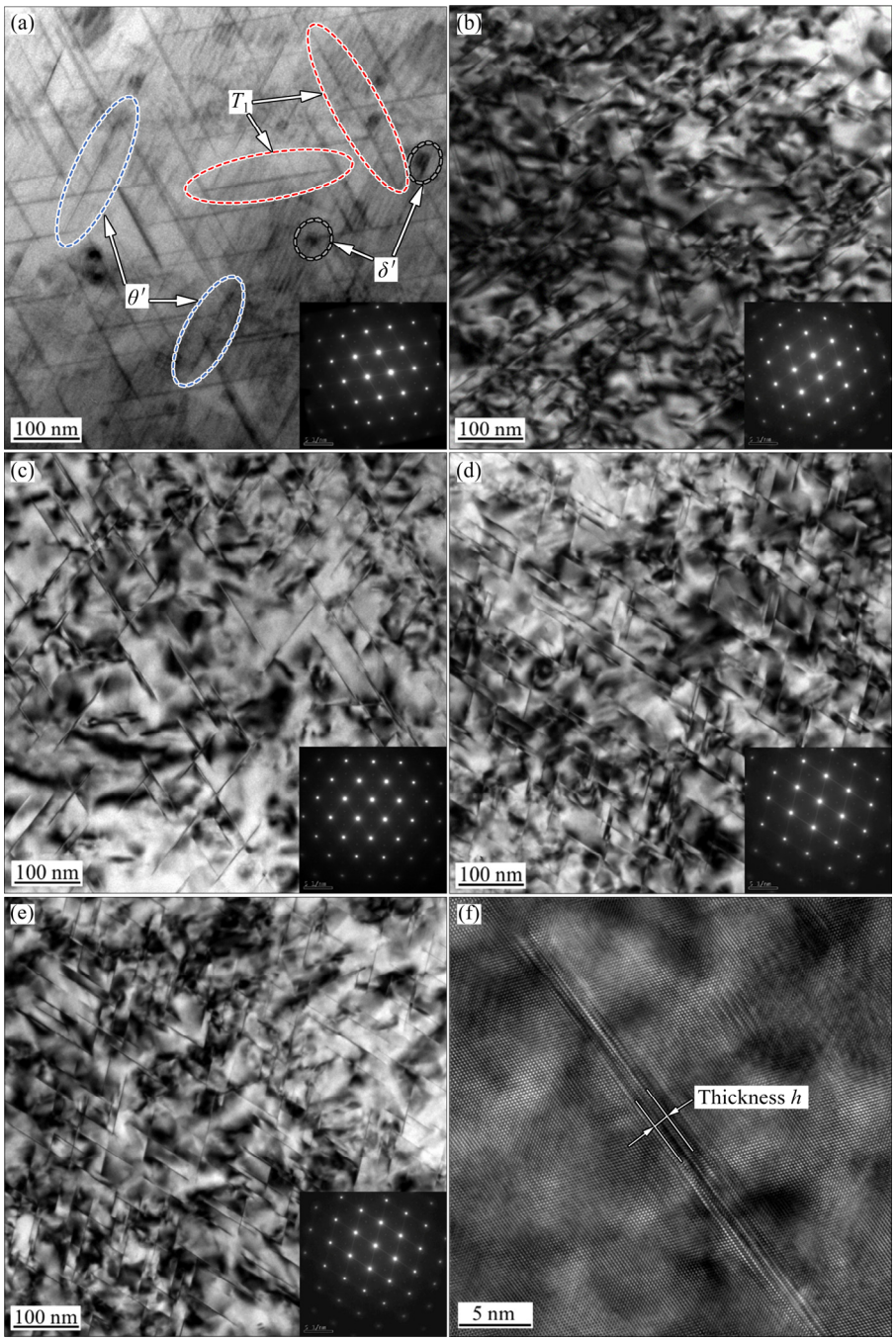

Fig. 10 Bright field TEM images and SAED patterns of different pre-deformed samples after CAF on $\langle 110\rangle_{Al}$ region axis: (a) Without pre-deformation; (b) 3% pre-stretching; (c) 3% pre-rolling; (d) 9% pre-stretching; (e) 9% pre-rolling; (f) T_1 phase HRTEM image

(the electron beam entered in the $\langle 110 \rangle_{Al}$ direction). As can be observed from Fig. 10, there is a significant difference among different pre-deformed specimens in the morphology of the T_1 phase. Figure 11(a) shows the variation of the average plate diameter of the T_1 phase with pre-deformation, in which the average plate diameters of the T_1 phase of the five types of specimens are 227, 113, 120, 71 and 80 nm, respectively. It is thus clear that, with the increase of the pre-deformation strain, the plate diameter of the T_1 phase declines, while the density of the T_1 phase increases. This is because the dislocation introduced by pre-deformation, as high-energy nucleation sites, can promote the heterogeneous nucleation and precipitation of the T_1 phase, that is, the higher the pre-deformation strain is, the more the nucleation sites there are. Furthermore, the limited quantities of the constituent elements Cu and Li result in the compact distribution and fine size of the T_1 phase. Besides, the massive precipitates of the T_1 phase will consume solute atoms Cu and Li, and thus inhibit both the θ' and δ' phases. It is apparent that θ' and δ' phases can be observed in Fig. 10(a), but in Figs. 10(b−e) after introducing pre-deformation, both of them are significantly reduced. As can be known from Fig. 7(a) and Fig. 10, with the increase of pre-deformation, the density of T_1 increases, while the contribution of precipitation presented a declining trend. This is because pre-deformation not only causes the increase of density of T_1, but also reduces the plate thickness h of the T_1 phase, as shown in Fig. 11(b). In this case, the reduction in the plate thickness of the T_1 phase weakens the obstruction of the dislocation motion, and its influence outweighs the influence of the increase in the number and density of the T_1 phase (which adds to the obstruction of the dislocation motion) [28,29]. In addition, according to the statistics in Fig. 11, among the specimens with same pre-deformation strain but different pre-deformation modes, there is certain difference in the size of the T_1 phase after creep aging; the plate diameter and thickness of the T_1 phase of the pre-stretched specimens are slightly lower than those of the pre-rolled specimens. For this reason, with the same pre-deformation strain, the pre-rolled specimens have a stronger precipitation strengthening effect than the pre-stretched specimens, as illustrated by the tensile properties at room temperature shown in Fig. 7(a).

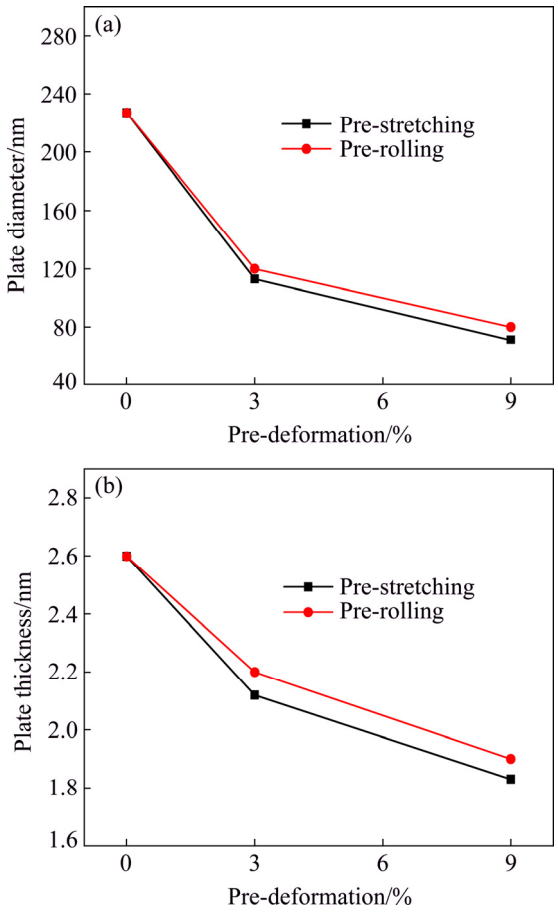

Fig. 11 T_1 phase size of different pre-deformed alloys after CAF: (a) Plate diameter; (b) Plate thickness

4 Conclusions

(1) Bending deformation method can effectively characterize the evolution laws of the creep strain of Al−Cu−Li alloy in the creep aging process, and intuitively embody the bending creep deformation effect. According to the bending creep test on panels, the creep strain first increases and then decreases with the increase of the pre-deformation strain; for the same pre-deformation strain, the creep strain values of the pre-rolled specimens are slightly lower than those of the pre-stretched specimens.

(2) Relative to the Al−Cu−Li alloy panel specimens without pre-deformation, the pre-deformed ones have better mechanical properties after CAF. When the pre-deformation strain increases from 3% to 9%, the Al−Cu−Li alloy panels show slightly increased strength properties, reduced elongation, and reduced Kahn tearing toughness and fatigue resistance properties after CAF.

(3) As indicated by the comparison of the Al−Cu−Li alloy panel specimens after CAF with different pre-deformation modes and strains, the pre-rolled specimens produce a work hardening effect that is slightly weaker than that produced by the pre-stretched specimens, but they also create a stronger aging-strengthening effect, so that the strength, toughness and fatigue resistance can all be improved to some extent. Among all types of specimens, the specimen with pre-deformation of 3% rolling has the best comprehensive mechanical properties after CAF.

References

[1] HOLMAN M C. Autoclave age forming large aluminum aircraft panels [J]. Journal of Mechanical Working Technology, 1989, 20: 477−488.

[2] ZHU A W, STARKE E A Jr. Materials aspects of age-forming of Al–*x*Cu alloys [J]. Journal of Materials Processing Technology, 2001, 117(3): 354−358.

[3] JEUNECHAMPS P P, HO K C, LIN J, PONTHOT J P, DEAN T A. A closed form technique to predict springback in creep age-forming [J]. International Journal of Mechanical Sciences, 2006, 48(6): 621−629.

[4] DECREUS B, DESCHAMPS A, de GEUSER F, DONNADIEU P, SIGLI C, WEYLAND M. The influence of Cu/Li ratio on precipitation in Al−Cu−Li−X alloys [J]. Acta Materialia, 2013, 61(6): 2207−2218.

[5] LAVERNIA E J, GRANT N J. Aluminum−lithium alloys [J]. Journal of Materials Science, 1987, 22(5): 1521−1529.

[6] RIOJA R J, LIU J. The evolution of Al−Li base products for aerospace and space applications [J]. Metallurgical and Materials Transactions A, 2012, 43(9): 3325−3337.

[7] LEQUEU P, SMITH K P, DANIÉLOU A. Aluminum−copper−lithium alloy 2050 developed for medium to thick plate [J]. Journal of Materials Engineering and Performance, 2010, 19(6): 841−847.

[8] KUMAR K S, BROWN S A, PICKENS J R. Effect of a prior stretch on the aging response of an Al−Cu−Li−Ag−Mg−Zr alloy [J]. Scripta Metall Mater, 1990, 24: 1245−1250.

[9] YOSHIMURA R, KONNO T J, ABE E, HIRAGA K. Transmission electron microscopy study of the evolution of precipitates in aged Al−Li−Cu alloys: The θ' and T_1 phases [J]. Acta Materialia, 2003, 51(14): 4251−4266.

[10] LI Jin-feng, HUANG Jia-lei, LIU Dan-yang, CHEN Yong-lai, ZHANG Xu-hu. Distribution and evolution of aging precipitates in Al−Cu−Li alloy with high Li concentration [J]. Transactions of Nonferrous Metals Society of China, 2019, 29(1): 15−24.

[11] NOBLE B, THOMPSON G E. T_1 (Al_2CuLi) precipitation in aluminum–copper–lithium alloys [J]. Metal Science Journal, 1972, 6(1): 167−174.

[12] CASSADA W A, SHIFLET G J, STARKE E A. The effect of plastic deformation on Al_2CuLi (T_1) precipitation [J]. Metallurgical Transactions A, 1991, 22(2): 299−306.

[13] GABLE B M, ZHU A W, CSONTOS A A, STARKE JR E A. The role of plastic deformation on the competitive microstructural evolution and mechanical properties of a novel Al−Li−Cu−X alloy [J]. Journal of Light Metals, 2001, 1(1): 1−14.

[14] LIN Yi, LU Chan-ge, WEI Cheng-yang, ZHEN Zi-qiao. Effect of aging treatment on microstructures, tensile properties and intergranular corrosion behavior of Al−Cu−Li alloy [J]. Materials Characterization, 2018, 141: 163−168.

[15] ZHANG Jin, WANG Cheng, ZHANG Yong, DENG Yun-lai. Effects of creep aging upon Al−Cu−Li alloy: Strength, toughness and microstructure [J]. Journal of Alloys and Compounds, 2018, 764: 452−459.

[16] LIU Fei, LIU Zhi-yi, LIU Meng, HU Yang-cheng, CHEN Ye, BAI Song. Analysis of empirical relation between microstructure, texture evolution and fatigue properties of an Al−Cu−Li alloy during different pre-deformation processes [J]. Materials Science and Engineering A, 2018, 726: 309−319.

[17] STARKE E A Jr, STALEY J T. Application of modern aluminum alloys to aircraft [J]. Progress in Aerospace Sciences, 1996, 32(2−3): 131−172.

[18] YING Pu-you, LIU Zhi-yi, BAI Song, LIU Meng, LIN Liang-hua, XIA Peng, XIA Lin-yan. Effects of pre-strain on Cu−Mg co-clustering and mechanical behavior in a naturally aged Al−Cu−Mg alloy [J]. Materials Science and Engineering A, 2017, 704: 18−24.

[19] HUANG Tian-tian, ZHAO Qi, LIU Zhi-yi, BAI Song. Enhanced damage tolerance through reconstructing residual stress and Cu−Mg co-clusters by pre-rolling in an Al−Cu−Mg alloy [J]. Materials Science and Engineering A, 2017, 700: 241−249.

[20] LI Y, SHI Z, YANG Y L, RONG Q, SAID R, SAILLARD P. Effects of asymmetric creep-ageing behaviour on springback of AA2050-T34 after creep age forming [J]. Procedia Engineering, 2017, 207: 287−292.

[21] LI Y, SHI Z, LIN J, YANG Y L, RONG Q, HUANG B M, CHUNG T F, TSAO C S, YANG J R, BALINT D S. A unified constitutive model for asymmetric tension and compression creep-ageing behaviour of naturally aged Al−Cu−Li alloy [J]. International Journal of Plasticity, 2017, 89: 130−149.

[22] ZHANG Jin, DENG Yun-lai, LI Si-yu, CHEN Ze-yu, ZHANG Xin-ming. Creep age forming of 2124 aluminum alloy with single/double curvature [J]. Transactions of Nonferrous Metals Society of China, 2013, 23(7): 1922−1929.

[23] JESHVAGHANI R A, EMAMI M, SHAHVERDI H R, HADAVI S M M. Effects of time and temperature on the creep forming of 7075 aluminum alloy: Springback and mechanical properties [J]. Materials Science and Engineering A, 2011, 528: 8795−8799.

[24] JESHVAGHANI R A, ZOHDI H, SHAHVERDI H R, BORZORG M, HADAVI S M M. Influence of multi-step heat treatments in creep age forming of 7075 aluminum alloy: Optimization for springback, strength and exfoliation corrosion [J]. Materials Characterization, 2012, 73: 8−15.

[25] JESHVAGHANI R A, SHAHVERDI H R, HADAVI S M M. Investigation of the age hardening and operative deformation mechanism of 7075 aluminum alloy under creep forming [J]. Materials Science and Engineering A, 2012, 552: 172−178.
[26] YANG You-liang, ZHAN Li-hua, LI Jie. Constitutive modeling and springback simulation for 2524 aluminum alloy in creep age forming [J]. Transactions of Nonferrous Metals Society of China, 2015, 25(9): 3048−3055.
[27] ZHANG Shao-shi, ZHANG Gui-lian, WANG Chun-xiang. New material mechanics [M]. 2nd ed. Beijing: China Machine Press, 2009. (in Chinese)
[28] RODGERS B I, PRANGNELL P B. Quantification of the influence of increased pre-stretching on microstructure-strength relationships in the Al−Cu−Li alloy AA2195 [J]. Acta Materialia, 2016, 108: 55−67.
[29] DESCHAMPS A, DECREUS B, de GEUSER F, DORIN T, WEVLAND M. The influence of precipitation on plastic deformation of Al−Cu−Li alloys [J]. Acta Materialia, 2013, 61(11): 4010−4021.

预变形方式及应变对 Al−Cu−Li 合金蠕变时效弯曲成形过程的影响

唐建国[1]，余 博[1]，张 劲[1,2]，胥福顺[3,4]，包崇军[3,4]

1. 中南大学 轻合金研究院，长沙 410083；
2. 中南大学 高性能复杂制造国家重点实验室，长沙 410083；
3. 昆明冶金研究院，昆明 650031；
4. 共伴生有色金属资源加压湿法冶金技术国家重点实验室，昆明 650031

摘 要：在一系列蠕变时效成形试验(CAF)的基础上，采用弯曲变形方法表征 Al−Cu−Li 合金在蠕变时效成形过程中的蠕变变形行为，并研究其在不同预变形条件下的力学性能和显微组织演变规律。结果表明，弯曲蠕变应变表征方法能直观地描述合金在 CAF 过程中蠕变变化。随着预变形应变的增加，试样的蠕变应变先增大后减小。预变形应变的增加能促进时效析出过程，提高成形合金的室温拉伸性能、Kahn 撕裂性能和疲劳扩展性能。与预拉伸试样样相比，预轧制试样产生稍弱的加工硬化，但也产生较强的时效强化效应，因此，其强度、韧性和损伤性能均有一定程度的提高。在所有类型的试样中，3%轧制试样经 CAF 处理后的综合力学性能最好。

关键词：Al−Cu−Li 合金；蠕变时效成形；预变形；弯曲蠕变应变；显微组织演变；力学性能

(Edited by Wei-ping CHEN)